Applied Surface Science 687 (2025) 162250

Contents lists available at ScienceDirect

Applied Surface Science

journal homepage: www.elsevier.com/locate/apsusc

Full Length Article

# Defect passivation and enhanced UV emission in β-$Ga_2O_3$ via remote fluorine plasma treatment

Amar K. Salih [a], Saskia Fiedler [b], Curtis P. Irvine [a], Fatima Matar [a], Matthew R. Phillips [a], Cuong Ton-That [a,*]

[a] School of Mathematical and Physical Sciences, University of Technology Sydney, Ultimo, New South Wales 2007, Australia
[b] Center for Nanophotonics, NWO-Institute AMOLF, Science Park 104, 1098 XG Amsterdam, the Netherlands

ARTICLE INFO

*Keywords:*
β-$Ga_2O_3$ nanowires
Fluorine doping
Defect passivation
Carrier dynamics
Hyperspectral imaging

ABSTRACT

This study investigates the incorporation of fluorene (F) donors in β-$Ga_2O_3$ and its effects on luminescence, defect structure and carrier dynamics. Monoclinic β-$Ga_2O_3$ nanowires (NWs) are synthesized via chemical vapour deposition and subsequently doped with F using remote $SF_6$ plasma treatment, leveraging their nanoscale cross sections. Photoelectron spectroscopy reveals F incorporation at oxygen sites and the formation of strong Ga–F bonds without sulfur contamination, while the monoclinic crystal structure remains intact. The impact of F doping is assessed using hyperspectral cathodoluminescence (CL) mapping and time-resolved spectroscopy of individual NWs. The β-$Ga_2O_3$ NWs exhibit a strong characteristic UV peak at 3.40 eV, associated with self-trapped holes, and visible defect-related emissions. After F incorporation, an additional UV emission at 3.64 eV emerges, attributed to shallow F donor-deep acceptor pair recombination, while the defect-related emissions are strongly supressed as F atoms occupy oxygen vacancies. Carrier lifetime increases from 9.2 ns to 17.0 ns with increasing F concentration along the nanowire. The work highlights the utility of F plasma processing to passivate intrinsic defects in $Ga_2O_3$ and the influence of F donors on the UV emission of β-$Ga_2O_3$.

## 1. Introduction

Monoclinic β-$Ga_2O_3$ is currently attracting significant attention as an emerging semiconductor due to its exceptional properties, including a large bandgap of 4.9 eV, an extremely high breakdown field of ~ 8 MV/cm, high electron mobility and remarkable thermal stability. This unique combination of physical and material properties makes β-$Ga_2O_3$ a strong candidate for the development of the next generation opto-electronic devices, with potential applications in UV transparent electrodes, solar-blind photodetectors, field-effect transistors, deep UV emitters as well as spintronic and power electronics [1–3]. The ultra-high breakdown field of β-$Ga_2O_3$ and suitability for mass production makes β-$Ga_2O_3$ especially useful for the development of energy efficient, low-cost high-power devices, potentially exceeding the performance of the currently employed electronics that utilize SiC and GaN based technologies.

Doping electronic oxides such as $Ga_2O_3$ presents challenges such as compensation effects, solubility limitations and defect formation. These oxides typically exhibit conductivity asymmetry, favouring n-type behavior. While initial theoretical studies proposed that unintentional n-type doping in $Ga_2O_3$ could be linked to oxygen vacancies ($V_O$), Varley *et al.* [4] used hybrid density function theory (DFT) calculations to demonstrate that $V_O$ acts as a deep donor and does not contribute to n-type conductivity. Furthermore, other studies reinforce the view that most native defects and their complexes have minimal impact on electrical conductivity [5,6]. Dopants such as silicon, zinc, nitrogen, tin, chlorine, and fluorine have been explored as possible shallow donors in $Ga_2O_3$ [5,7–10]. Group IV elements (Si, Ge, Sn) are expected to substitute Ga cation sites, while group VII elements (Cl, F) occupy O anion sites. The monoclinic structure of $Ga_2O_3$ contains two different Ga sites (tetrahedral $Ga_{(I)}$ and octahedral $Ga_{(II)}$) and three distinct tetrahedral oxygen sites (two three-fold coordinated $O_{(I)}$ and $O_{(II)}$, and one with four-fold coordinated ($O_{(III)}$). DFT calculations show that on the Ga sites, Si and Ge prefer the $Ga_{(I)}$ site and Sn favors the $Ga_{(II)}$ site, whereas on the O anion sites Cl and F occupy the $O_{(I)}$ site [11]. Experimental studies have demonstrated that F doping significantly influences the electrical properties of β-$Ga_2O_3$-based devices. For instance, Jeong *et al.* [12] reported that F doping enhances ohmic contact formation in β-$Ga_2O_3$

* Corresponding author.
*E-mail address:* cuong.ton-that@uts.edu.au (C. Ton-That).

https://doi.org/10.1016/j.apsusc.2024.162250
Received 30 October 2024; Received in revised form 17 December 2024; Accepted 28 December 2024
Available online 30 December 2024
0169-4332/© 2024 The Author(s). Published by Elsevier B.V. This is an open access article under the CC BY license (http://creativecommons.org/licenses/by/4.0/).

MOSFETs, leading to reduced resistivity and contact resistance. Furthermore, F doping increases carrier concentration across the surface and bulk of the device. Theoretical studies further support these findings, revealing that F doping introduces n-type behavior in β-$Ga_2O_3$ and a progressive narrowing of the bandgap with increasing F concentration [13]. Collectively, these studies highlight the potential of F doping to tune the electrical properties of β-$Ga_2O_3$, expanding its application in electronic and optoelectronic devices.

β-$Ga_2O_3$ exhibits luminescence across the UV–visible spectrum in both bulk and nanostructured forms [14,15]. The optical emission bands, spanning from 1.8 eV to 3.8 eV, strongly depend on sample morphology, growth conditions and doping. These emission peaks are categorized into four distinct spectral regions: UV, blue (BL), green (GL), and red (RL) luminescence [15–17]. Notably, a near-band-edge (NBE) emission is absent in β-$Ga_2O_3$ due to the rapid formation of self-trapped holes (STHs), which radiatively recombine to produce an UV emission [18,19]. In nominally undoped β-$Ga_2O_3$ crystals, UV emission dominates at low temperatures, whereas BL, GL and RL bands become prevalent at room and elevated temperatures due to the thermalization of self-trapped excitons [15,16]. The visible peaks are associated with native defects, such as oxygen ($V_O$) and gallium ($V_{Ga}$) vacancies [14], as well as donor–acceptor pairs (DAPs) involving acceptors like $V_{Ga}$ and $V_{Ga}$–$V_O$ complexes [16].

This study investigates the effects of $SF_6$ plasma treatment on the doping of $Ga_2O_3$ nanowires (NWs) and elucidates the interactions between fluorine species (atoms, radicals generated by $SF_6$ plasma dissociation) and native defects in β-$Ga_2O_3$ NWs. We provide fundamental insights into fluorine passivation mechanisms in β-$Ga_2O_3$, showing that F can substitute oxygen atoms and occupy $V_O$ sites, where it interacts with Ga dangling bonds. Additionally, due to their high electronegativity, fluorine anions on the $Ga_2O_3$ surface may attract hydrogen atoms, promoting the formation of intermolecular hydrogen F-OH bonds. Passivating oxygen vacancies by fluorine atom occupation and reducing the number of dangling Ga bonds can significantly improve $Ga_2O_3$ device performance by decreasing the density of carrier trap states.

## 2. Materials and methods

β-$Ga_2O_3$ NWs were synthesized on Au-coated Si(100) substrates via the chemical vapour deposition (CVD) method. A 5 nm Au layer was coated on Si(100) substrate using a sputter coated. The substrate and high-purity Ga (99.99 %) source were placed in a quartz tube and heated to 850 °C for 30 min at ~ 1 Torr pressure. A constant flow of Ar at 200 sccm and $O_2$ at 2 sccm, controlled by a mass flow controller (MFC), transported the Ga precursor to the substrate, facilitating the growth of $Ga_2O_3$ nanowires (NWs). F-doping was achieved by exposing the NWs to $SF_6$ gas using an inductively coupled plasma (ICP) system. During this process, the $SF_6$ gas flow was maintained at 30 sccm, while the RF power was set to 300 W to ionize the gas. The bias power was kept at zero to minimize etching effects. The $SF_6$ plasma treatment was conducted for 2 h. The fabrication steps for F-doped $Ga_2O_3$ nanowires (F:$Ga_2O_3$ NWs) are illustrated in Scheme 1, which outlines the growth of $Ga_2O_3$ NWs via CVD followed by fluorine doping using $SF_6$ remote plasma treatment.

Both untreated and F-doped $Ga_2O_3$ (F:$Ga_2O_3$) NWs were characterized using a range of analytical techniques. A Zeiss Supra 55VP field emission scanning electron microscope (SEM) equipped with an Oxford Instruments EDS was used for morphological and elemental analysis. The crystal structure was confirmed using a Bruker D8 Discovery X-ray diffractometer (XRD) with Cu Kα radiation, employing a 0.02° scanning step. X-ray photoelectron spectroscopy (XPS) was performed on the Soft X-ray Spectroscopy (SXS) beamline at the Australian Synchrotron. Cathodoluminescence (CL) spectroscopy was conducted using a FEI Quanta FEG 650 SEM (Thermo Fisher Scientific Inc., MA, USA). CL spectra were collected by a parabolic mirror and analyzed with a Delmic SPARC CL detector coupled with an Andor Newton charge-coupled device (CCD) camera. Hyperspectral CL maps were acquired with a 5 keV electron beam, a beam current of 85 pA and 100 ms acquisition time. For the time-resolved CL (TR-CL) measurements, an electrostatic beam blanker together with a 70 μm aperture was inserted to generate pulsed electron beam excitation with a pulse duration of approximately 90 ps [20].

## 3. Results and discussion

SEM images of the $Ga_2O_3$ NWs are presented in Fig. 1(a). The NWs are densely populated and uniformly distributed across an entire 10 × 10 $mm^2$ area of the substrate, exhibiting NW lengths of a few tens of microns and diameters ranging from 300 to 500 nm. EDS elemental mapping and spectra are shown in Fig. 1(b, c). Upon $SF_6$ plasma treatment, the EDS elemental mapping of single nanowires reveals that the F distribution is spatially correlated with that of Ga atoms, confirming successful F incorporation throughout the $Ga_2O_3$ NWs [Fig. 1(b)]. Additionally, the EDS spectra of the NWs show characteristic Ga and O X-ray peaks, along with an F peak following the $SF_6$ plasma treatment. The absence of Au is consistent with the growth model for a combined vapour–solid (VS) and vapour–liquid–solid (VLS) mechanism [21]. Moreover, upon $SF_6$ ionization inside the ICP chamber, $SF_x^-$ ions and F radicals are produced and subsequently adsorbed by the $Ga_2O_3$ NWs. This process results in formation of non-volatile $GaF_x$ on the surface, while the vaporized S $O_y$ species are exhausted. The reaction between $Ga_2O_3$ NWs and $SF_6$ can be described by the following equation: $Ga_2O_3 + SF_6 = GaF_x(s) + SO_y(g)$ [22]. This explains the absence of sulfur (S) in the EDS results and the formation of S-free F:$Ga_2O_3$ NWs, consistent with previous observations for other materials doped via $SF_6$ plasma treatment [23,24]. The incorporation of F radicals along the NW length is not uniformed. The EDS spectra of the F:$Ga_2O_3$ NWs reveal a gradual increase in the intensity ratio of the F to Ga X-ray peaks from the NW root and the tip (Fig. S1). This indicates that the fluorine incorporation is highest at the tip, followed by the middle, and lowest at the root of the NW.

Fig. 1(d) presents the XRD patterns of $Ga_2O_3$ and F:$Ga_2O_3$ NWs, confirming the growth of high-quality monoclinic β-$Ga_2O_3$, consistent

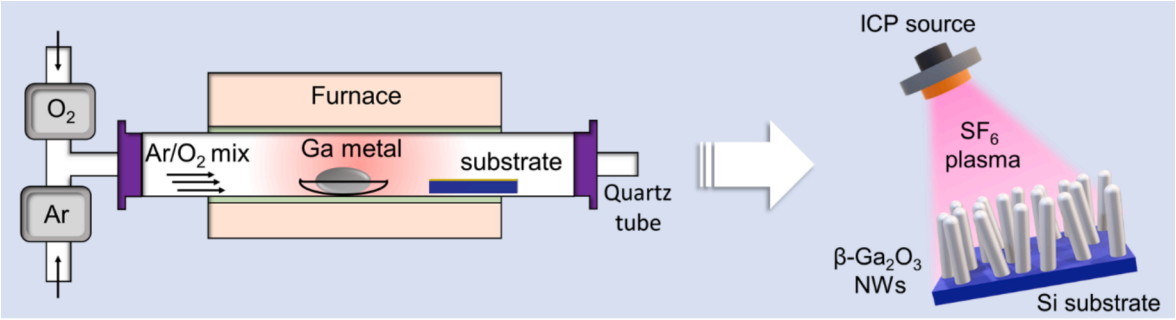


**Scheme 1.** Schematic representation of the procedure for the growth of $Ga_2O_3$ NWs by CVD and subsequent F doping using $SF_6$ remote plasma.

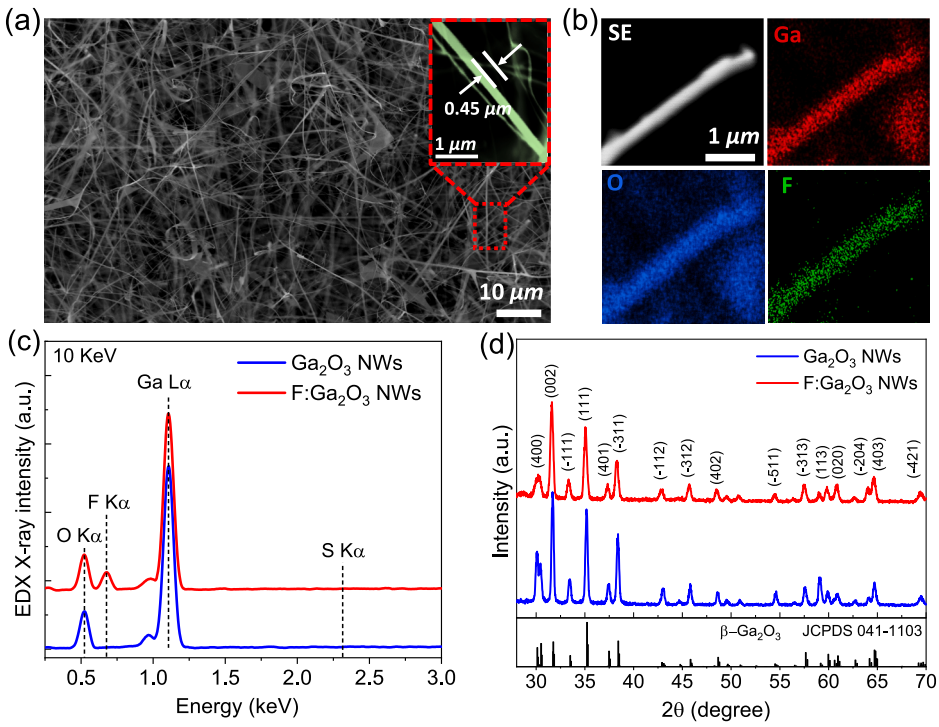


**Fig. 1.** (a) SEM image of $Ga_2O_3$ NWs grown over an entire area of 10 × 10 $mm^2$, with an average NW diameter ranging from 300 to 500 nm. (b) SEM image and corresponding EDS elemental maps of Ga, O, and F for an individual F-doped NW, showing the incorporation of fluorine along the NW length. (c) EDS spectra of the NWs, showing the characteristic F Kα X-ray peak at 0.70 keV in F:$Ga_2O_3$ NWs, while the S Kα X-ray peak at 2.3 eV is completely absent. (d) XRD patterns of $Ga_2O_3$ and F:$Ga_2O_3$ NWs with all peaks indexed to the β-$Ga_2O_3$ monoclinic structure.

with previous reports [25]. No additional peaks corresponding to any impurity phases, such as $GaF_3$, are detected in the XRD pattern of F:$Ga_2O_3$ [26], indicating that F is primarily incorporated into the $Ga_2O_3$ lattice. However, the existence of a nanoscale $GaF_x$ surface layer is possible as it would most likely be too thin to produce detectable XRD peaks. While XRD peaks along the (002), (111), and (−311) planes are prominent, no preferred orientation can be discerned, indicating that the NWs grow randomly with respect to the substrate normal. The XRD patterns of the $Ga_2O_3$ and F:$Ga_2O_3$ NWs are nearly identical, with only slight variations in relative peak intensities, confirming that the F incorporation does not induce secondary phases and has a minimal impact on the crystalline quality of the NWs.

XPS measurements conducted on the $Ga_2O_3$ and F:$Ga_2O_3$ NWs confirm the incorporation of fluorine into $Ga_2O_3$ NWs. Survey spectra acquired at a photon energy $h\nu = 1486.6$ eV for $Ga_2O_3$ and F:$Ga_2O_3$ NWs [Fig. 2(a)] show the characteristic photoelectron and Auger peaks for Ga and O, with an additional F 1 s peak at 683.2 eV in the F:$Ga_2O_3$ spectrum, confirming successful fluorine doping. Importantly, no sulfur contamination is detected, as evidenced by the absence of S 2p (at ~ 164 eV) and S 2 s (~ 225 eV) signals, corroborating the EDS results. Fig. 2(b) shows the Ga 2p spectrum for $Ga_2O_3$ NWs, fitted with two doublet peaks at 1117.8 eV (Ga $2p_{3/2}$) and 1144.9 eV (Ga $2p_{1/2}$), with an energy separation of 27.1 eV, consistent with Ga–O bonds of β-$Ga_2O_3$ [27]. For F:$Ga_2O_3$ NWs [Fig. 2c], additional doublet peaks appear at 1120.8 eV and 1147.6 eV indicate the formation of Ga–F bonds, confirming the incorporation of fluorine into the $Ga_2O_3$ NWs [28]. Theoretical studies show that the formation energy of interstitial fluorine ($F_i$) is significantly higher than that of substitutional fluorine ($F_O$) [29], suggesting that fluorine is primarily incorporated by substituting O atoms or by occupying oxygen vacancies ($V_O$), rather than forming interstitial configurations. Due to the similar ionic radii of fluorine and oxygen, fluorine can integrate into the $Ga_2O_3$ lattice with minimal structural distortion [30]. Surface-sensitive XPS at $h\nu = 120$ eV further reveals heavy fluorination at the NW surface. Fig. S2 presents the valence band (VB) spectra for $Ga_2O_3$ and the Ga 3d core level, corresponding to Ga-O bonding [31]. In F:$Ga_2O_3$ NWs, a new peak at 24.8 eV emerges, attributed to the formation of Ga–F bonds. The F doping also induces a notable shift in the VB onset from 3.2 eV to 2.5 eV, which is likely due to the formation of $F_O$ shallow donors in the $Ga_2O_3$ NWs. This VB shift may also arise from to the passivation of surface states by fluorine [28]. The F incorporation into NWs is confirmed by the XPS spectra acquired at photon energies of 1486.6 and 120 eV (Figs. 2 and S2), corresponding to sampling depths of 7.2 nm and 1.5 nm, respectively [32]. These results indicates that fluorine is distributed throughout the near-surface and sub-surface regions of the NWs. The O 1s core level spectra of $Ga_2O_3$ and F:$Ga_2O_3$ NWs are shown in Fig. 2(d, e). The O 1s spectrum is deconvoluted into two peaks at 530.6 eV [$O_{(I)}$] and 532.2 eV [$O_{(II)}$], attributed to Ga–O bonds and surface –OH groups, respectively [30]. The increased intensity of $O_{(II)}$ in F:$Ga_2O_3$ NWs indicates enhanced adsorption of –OH groups, likely due to the high electronegativity of fluorine, which can attract hydrogen, resulting in the formation of intermolecular F–HO hydrogen bonds [28]. The F 1s spectrum of F:$Ga_2O_3$ NWs, presented in Fig. 2(f), reveals two Gaussian-fitted components at 685.9 and 688.6 eV. The peak at 685.9 eV corresponds F–Ga bonds, while the higher-energy peak at 688.6 eV is attributed to F–HO interactions [30,33].

The effects of fluorine incorporation on the luminescence properties of $Ga_2O_3$ are analyzed using hyperspectral CL imaging and spectroscopy analysis of individual NWs (Fig. 3). The CL spectrum of F:$Ga_2O_3$ remains stable even after 30 min of continuous 5 kV e-beam irradiation, indicating the robustness of the material. The F doping induces a notable blue shift in the CL emission, shifting from 3.24 eV for undoped $Ga_2O_3$ to 3.37 eV for F:$Ga_2O_3$. This 130 meV shift is attributed to the emergence of a new emission arising from F-related shallow donors, which can be analysed through Gaussian peak fitting as previously reported for β-$Ga_2O_3$ [34,35]. In monoclinic β-$Ga_2O_3$, the STH and defect-related CL peaks overlap significantly as both emissions are inherently broad due to strong electron-photon coupling, necessitating spectral deconvolution to

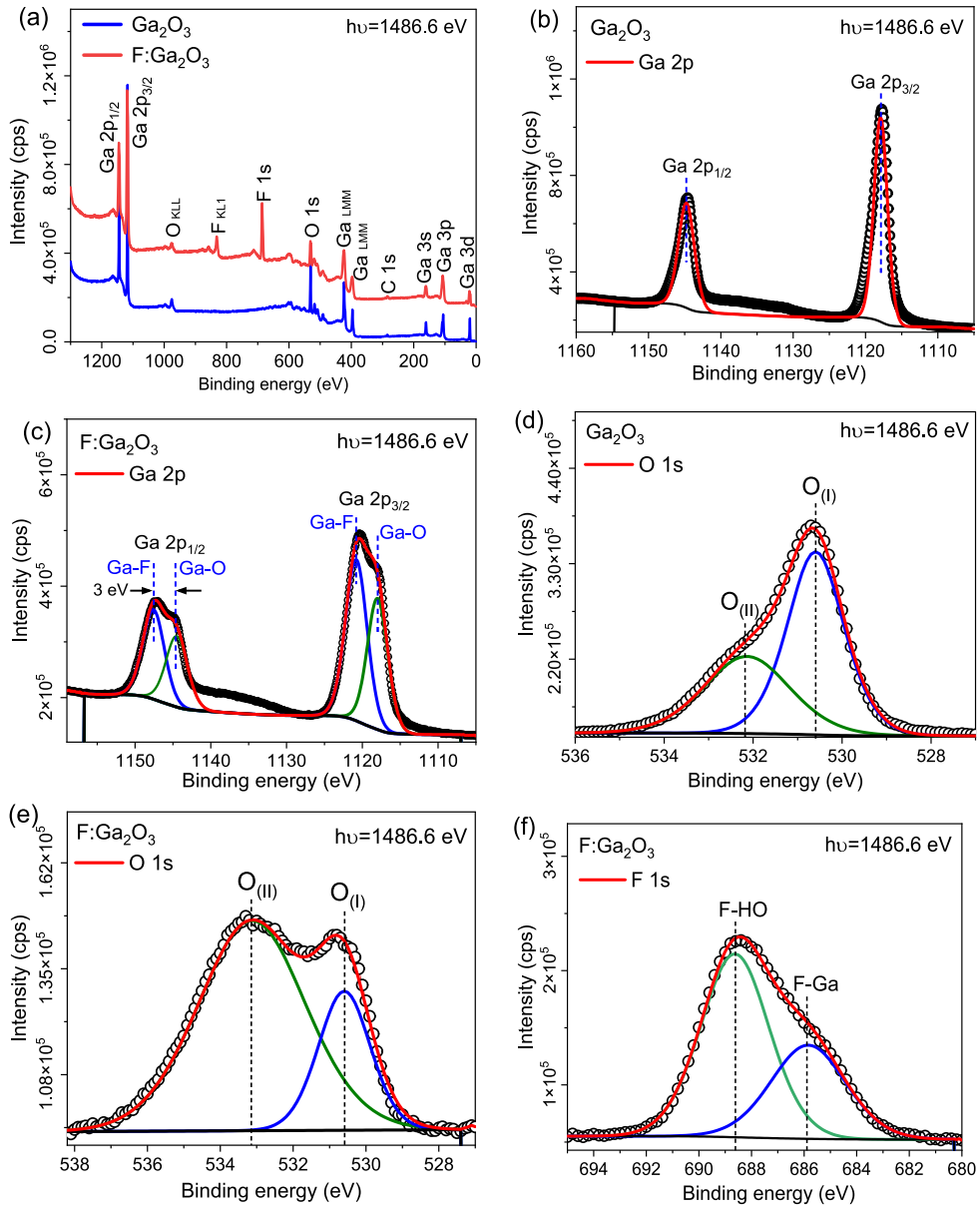


**Fig. 2.** (a) XPS survey spectra of $Ga_2O_3$ and F:$Ga_2O_3$ NWs acquired at h$\nu$ = 1486.6 eV, showing a pronounced F 1 s peak after the plasma doping, with no detectable sulfur signals. (b, c) Ga 2p core level spectra revealing the formation of Ga–F bonds. (d, e) O 1 s spectra deconvoluted into two peaks assigned to O–Ga bonds [$O_{(I)}$] and oxygen–hydroxyl (O–OH) bonds [$O_{(II)}$]. The $O_{(II)}$ intensity increases significantly in F:$Ga_2O_3$ NWs I attributed to –OH adsorption, driven by the high electronegativity of F ions. (f) F 1 s spectrum for F:$Ga_2O_3$, fitted into two peaks corresponding to F–Ga and F–HO bonds.

interpret the luminescence data meaningfully [15]. Applying this approach, the CL spectrum of $Ga_2O_3$ NWs is deconvoluted into three Gaussian peaks: UV, $BL_1$ and $BL_2$ [Fig. 3(b)]. In the fitting procedure, the STH peak is first fitted on the high-energy side at 3.40 eV using the peak position and FWHM consistent with the isolated STH emission in β-$Ga_2O_3$ [36]. The low-energy side of the luminescence spectrum is then fitted with two broad defect-related Gaussian peaks ($BL_1$ and $BL_2$) centred at 3.14 eV and 2.93 eV, respectively, each with an FWHM of approximately 0.64 eV. These values are consistent with previously reported CL data for β-$Ga_2O_3$ single crystals [34]. The two blue bands ($BL_1$ and $BL_2$) have been attributed to DAP radiative recombination channels involving deep $V_O$ donors and deep acceptors, such as isolated $V_{Ga}$ and $V_O$-$V_{Ga}$ defect pairs [15,16]. The relative intensity ratios of the three deconvoluted peaks are found to be $BL_1/UV = 0.72$ and $BL_2/UV = 0.34$.

For the F:$Ga_2O_3$ NWs, similar deconvolution shows three similar deconvoluted Gaussian peaks, plus an additional high-energy UV peak ($UV^+$) at 3.64 eV. This $UV^+$ emission is consistent with DAP recombination involving F shallow donors and deep acceptors [37], as revealed by the XPS results showing the formation of substitutional $F_O$ dopants post-doping. Indeed, the relative intensity ratios of $BL_1$/UV and $BL_2$/UV peaks in F:$Ga_2O_3$ NW decrease to 0.42 and 0.20, respectively, indicating a significant reduction in defect-related emission. This reduction indicates the passivation of native defects, such as $V_O$, after fluorine incorporation, which have been observed in previous studies [24,28]. The passivation of $V_O$ defects by F is significant as it may reduce background n-type conductivity associated with $V_O$-related donors as previously reported [38]. Additionally, a slight reduction in the overall luminescence intensity is observed after F doping, as shown in Fig. S3. This reduction is likely caused by changes in the surface recombination velocity in F:$Ga_2O_3$ NWs. Fig. 3(d) summarizes the CL emission pathways for $Ga_2O_3$ and F:$Ga_2O_3$ NWs. For undoped NWs, the emission channels include the radiative recombination through the STH state (UV band) and DAP transitions ($BL_1$ and $BL_2$ bands). A similar recombination model is applicable to F-doped NWs, with the addition of the $UV^+$

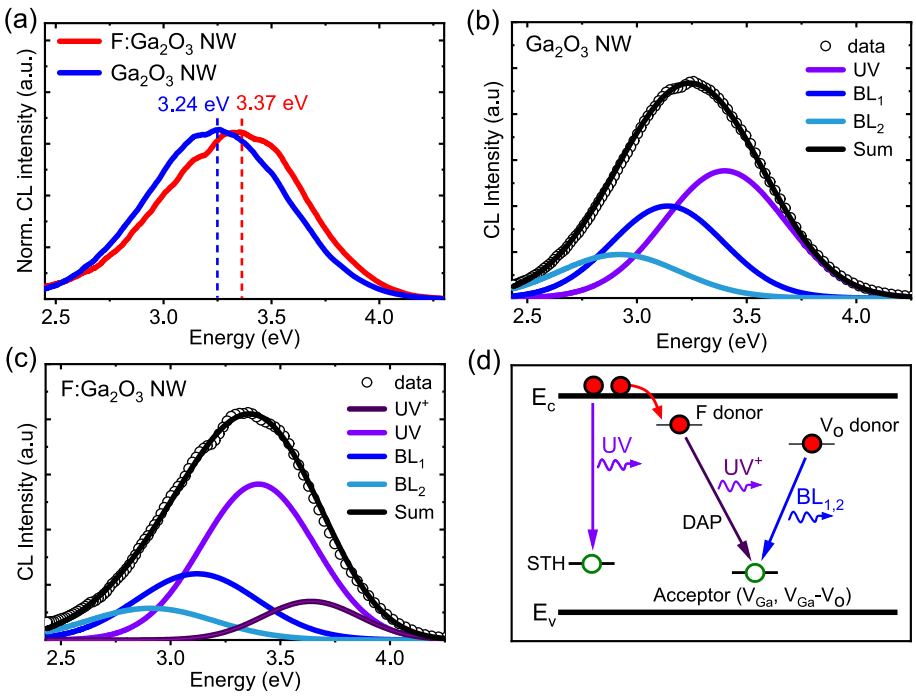


**Fig. 3.** (a) Normalized CL spectra of $Ga_2O_3$ and F:$Ga_2O_3$ NWs acquired under identical excitation conditions (5 kV and 85 pA). The F doping induces a blue shift of 0.13 eV in the luminescence spectrum. (b, c) CL spectral deconvolution for $Ga_2O_3$ and F:$Ga_2O_3$, revealing three luminescence bands: UV at 3.40 eV, $BL_1$, and $BL_2$, and an additional higher-energy band at 3.64 eV ($UV^+$) emerging after F doping. Both $BL_1$ at 3.14 eV and $BL_2$ at 2.93 eV decrease in relative intensity in F:$Ga_2O_3$ NWs. (d) Schematic emission model for $Ga_2O_3$ and F:$Ga_2O_3$ NWs, showing radiative recombination through the STH (UV band), DAP transitions ($BL_1$ and $BL_2$ bands), and DAP involving F donors ($UV^+$ band).

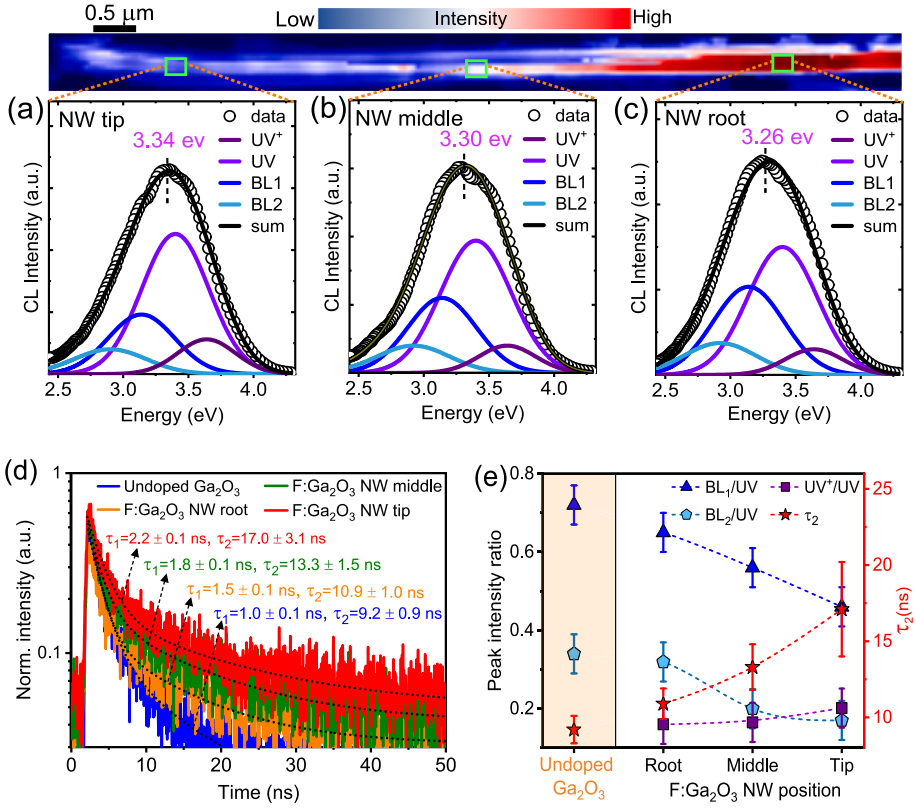


**Fig. 4.** (a, b, c) CL spectra of a single F:$Ga_2O_3$ NW acquired from an 100 × 100 nm area at the tip, middle and root regions, based on the hyperspectral CL map of the NW displayed above. (d) Corresponding TR-CL decay curves with the dashed lines representing bi-exponential decay fits. For the undoped NW, the decay times are $\tau_1 = 1.0 \pm 0.1$ ns and$\tau_2 = 9.2 \pm 0.9$ ns. After F doping, both decay times increase significantly, with $\tau_1 = 2.2 \pm 0.1$ ns and$\tau_2 = 17.0 \pm 3.1$ ns at the F:$Ga_2O_3$ NW tip. (e) Relative intensities of the defect-related BL and F-related $UV^+$ emissions compared to the intrinsic UV emission for undoped β-$Ga_2O_3$, and along the F:$Ga_2O_3$ NW length. The results reveal an anti-correlation between the defect emissions and $UV^+$ emission from the root to the tip of the F:$Ga_2O_3$ NW.

transition arising from shallow donor – deep acceptor DAP recombination involving F donors. Neither undoped nor F-doped NWs exhibit an NBE emission, indicating the absence of minority free holes in the VB, in agreement with the rapid self-trapping of holes in β-$Ga_2O_3$.

The influence of F doping on $Ga_2O_3$ is further investigated by hyperspectral CL mapping of individual NWs with a pixel size of 50 × 50 nm. In Fig. 4 (a-c), CL spectra from three different regions along the NW, i.e. root, middle, and tip, averaged over an area of 100 × 100 nm for each region are selected to illustrate spectral changes within a single NW. A gradual reduction in $BL_1$ and $BL_2$ emissions, coupled with an increase in the $UV^+$ emission, is observed from the root to the tip, indicating a gradient in F doping concentration along the NW length. Notably, the CL peak gradually shifts from 3.34 eV at the tip to 3.26 eV at the root of the NW, reflecting the suppression of defect-related emissions and the emergence of $UV^+$ emission associated with the higher F concentration in the tip region. This trend aligns with the variation in the intensity ratio of the F to Ga X-ray peaks (Fig. S1), which confirms an increased fluorine concentration at the NW tip compared to the middle and root NW regions. It is also noteworthy that the overall CL emission intensity is higher at the NW root and gradually decreases along its length, as shown in the hyperspectral CL map in Fig. 4. This reduction in intensity reflects an increased density of non-radiative defects formed during the NW growth.

The impact of F doping on the carrier dynamics is further investigated using TR-CL measurements, as depicted in Fig. 4 (d). The CL emission decay curves are fitted using a bi-exponential function, represented by the dashed lines, defined as $I(t) = I_o + I_1\exp\left(\frac{-t}{\tau_1}\right) + I_2\exp\left(\frac{-t}{\tau_2}\right)$, where $\tau_1$ and $\tau_1$ are decay time constants, $I_1$ and $I_2$ represent the intensities of the decay components, and $I_o$ denotes the background signal. The fast decay component $\tau_1$, typically between 1 and 3 ns, is commonly observed in various $Ga_2O_3$ materials and has been attributed to surface recombination of carriers [39,40]. The F doping is found to extend the charge carrier lifetime, affecting both the fast and slow decay components. For undoped NWs, the fast decay component has $\tau_1 = 1.0 \pm 0.1$ ns, which increases to $\tau_1 = 2.2 \pm 0.1$ ns at the NW tip where the F doping concentration is highest. The increase in $\tau_1$ could be due to additional surface defects introduced by plasma treatment. Notably, the slow decay component, associated with the delayed recombination of carriers via STHs and defects, is extended from $\tau_2 = 9.2 \pm 0.9$ ns for undoped NWs to $\tau_2 = 17.0 \pm 3.1$ ns at the F-doped NW tip. These measurements suggest that the extended $\tau_2$ component results from carrier recombination through the F donor state [Fig. 3(d)], which is competitive with and slower than the STH recombination channel [41]. Furthermore, the $\tau_2$ lifetime decrease in the lower regions (middle and root) of the F-doped NW, correlating with a reduced number of donor states due to the lower F doping concentration. Fig. 4 (e) summarizes the relative intensities of defect-related and F-related emissions for $Ga_2O_3$ NW and along the F:$Ga_2O_3$ NW. The $UV^+$/UV ratio shows a slight increase from root to tip, consistent with a higher F concentration at the NW tip, which aligns with the expected dopant profile for plasma doping processes [42]. In contrast, both the $BL_1$/UV and $BL_2$/UV intensity ratios gradually decrease from 0.65 and 0.32 at the root to 0.46 and 0.17 at the tip, correlating with a decreasing F doping concentration. This indicates effective passivation of native defects by F ions during the remote plasma treatment. The higher F concentration towards the NW tip also results in extended carrier lifetimes, with the decay lifetime increasing from 10.9 ± 1.0 ns at the root to 17.0 ± 3.1 ns at the tip. These TR-CL findings highlight the effectiveness of $SF_6$ plasma processing in both passivating native defects and incorporating F shallow donors in $Ga_2O_3$, offering insights into the tunability of luminescence and carrier dynamics through F doping.

## 4. Conclusions

$Ga_2O_3$ NWs can be successfully doped with fluorine shallow donors using $SF_6$ remote plasma treatment. Fluorine is found to be incorporated along the entire length of the NWs, without any detectable sulfur contamination. Importantly, the NWs retain their monoclinic structure without deteriorating crystal quality after the plasma treatment, exhibiting the characteristic self-trapped hole emission. Photoemission spectroscopy reveals the formation of Ga–F bonds, accompanied by strong adsorption of –OH groups on the NW surface. The incorporation of fluorine effectively passivates native defects, as indicated by a marked reduction in defect-related luminescence. Moreover, a new UV emission band, located at 0.2 eV above the self-trapped hole emission, emerges post-treatment and is attributed to donor–acceptor-pair recombination involving F shallow donors and deep defect-related acceptors. This newly formed recombination channel leads to a significant increase in carrier lifetime, extending from 9.2 ± 0.9 ns in undoped $Ga_2O_3$ to 17.0 ± 3.1 ns in highly F-doped nanowires. These findings highlight the important role of F doping in modulating carrier dynamics and enhancing UV emission in β-$Ga_2O_3$, offering new insights for advancing deep UV optoelectronic applications.

## CRediT authorship contribution statement

**Amar K. Salih:** Writing – original draft, Visualization, Validation, Methodology, Investigation, Formal analysis, Data curation, Conceptualization. **Saskia Fiedler:** Methodology, Investigation. **Curtis P. Irvine:** Methodology, Investigation. **Fatima Matar:** Methodology, Investigation. **Matthew R. Phillips:** Writing – review & editing, Validation, Supervision. **Cuong Ton-That:** Writing – review & editing, Validation, Supervision, Funding acquisition, Formal analysis, Conceptualization.

## Declaration of competing interest

The authors declare the following financial interests/personal relationships which may be considered as potential competing interests: Cuong Ton-That reports equipment, drugs, or supplies and travel were provided by The Australian Synchrotron. Cuong Ton-That reports a relationship with Australian Research Council that includes: funding grants. If there are other authors, they declare that they have no known competing financial interests or personal relationships that could have appeared to influence the work reported in this paper.

## Acknowledgements

This research was partly conducted on the Soft X-ray Spectroscopy beamline at the Australian Synchrotron, Victoria, Australia. The work was supported by the Australian Research Council (ARC) Discovery Project funding scheme (Project DP210101146). The authors wish to thank Bruce Cowie, Anton Tadich, James Bishop and Herbert Yuan for their technical support.

## Appendix A. Supplementary data

Supplementary data to this article can be found online at https://doi.org/10.1016/j.apsusc.2024.162250.

## Data availability

Data will be made available on request.

## References

[1] D. Guo, Q. Guo, Z. Chen, Z. Wu, P. Li, W. Tang, Review of $Ga_2O_3$-based optoelectronic devices, Mater. Today Phys. 11 (2019) 100157.
[2] S. Pearton, J. Yang, P.H. Cary, F. Ren, J. Kim, M.J. Tadjer, M.A. Mastro, A review of $Ga_2O_3$ materials, processing, and devices, Appl. Phys. Rev. 5 (2018).

[3] D. Kaur, S. Debata, D.P. Singh, M. Kumar, Strain effects on the optoelectronic performance of ultra-wide band gap polycrystalline β-$Ga_2O_3$ thin film grown on differently-oriented Silicon substrates for solar blind photodetector, Appl. Surf. Sci. 616 (2023) 156446.
[4] J.B. Varley, J.R. Weber, A. Janotti, C.G. Van de Walle, Oxygen vacancies and donor impurities in β-$Ga_2O_3$, Appl. Phys. Lett. 97 (2010).
[5] M.D. McCluskey, Point defects in $Ga_2O_3$, J. Appl. Phys. 127 (2020).
[6] A. Kyrtsos, M. Matsubara, E. Bellotti, Migration mechanisms and diffusion barriers of vacancies in $Ga_2O_3$, Phys. Rev. B 95 (2017) 245202.
[7] A.T. Neal, S. Mou, S. Rafique, H. Zhao, E. Ahmadi, J.S. Speck, K.T. Stevens, J. D. Blevins, D.B. Thomson, N. Moser, Donors and deep acceptors in β-$Ga_2O_3$, Appl. Phys. Lett. 113 (2018).
[8] S. Kim, H.-Y. Kim, Y. Kim, D.-W. Jeon, W.S. Hwang, J.-H. Park, High-performance normally-off Si-doped β-$Ga_2O_3$ deep ultraviolet phototransistor grown on N-doped β-$Ga_2O_3$, Appl. Surf. Sci. 679 (2025) 161165.
[9] J. Yang, C. Fares, F. Ren, R. Sharma, E. Patrick, M.E. Law, S. Pearton, A. Kuramata, Effects of fluorine incorporation into β-$Ga_2O_3$, J. Appl. Phys. 123 (2018).
[10] M.J. Tadjer, J.L. Lyons, N. Nepal, J.A. Freitas, A.D. Koehler, G.M. Foster, Review—Theory and characterization of doping and defects in β-$Ga_2O_3$, ECS J. Solid State Sci. Technol. 8 (2019) Q3187–Q3194.
[11] R. Sharma, M.E. Law, F. Ren, A.Y. Polyakov, S.J. Pearton, Diffusion of dopants and impurities in β-$Ga_2O_3$, J. Vac. Sci. Technol. A 39 (2021).
[12] Y.J. Jeong, J.Y. Yang, C.H. Lee, R. Park, G. Lee, R.B.K. Chung, G. Yoo, Fluorine-based plasma treatment for hetero-epitaxial β-$Ga_2O_3$ MOSFETs, Appl. Surf. Sci. 558 (2021) 149936.
[13] J. Yan, C. Qu, Electronic structure and optical properties of F-doped β-$Ga_2O_3$ from first principles calculations, J. Semicond. 37 (2016) 042002.
[14] H. Gao, S. Muralidharan, N. Pronin, M.R. Karim, S.M. White, T. Asel, G. Foster, S. Krishnamoorthy, S. Rajan, L.R. Cao, Optical signatures of deep level defects in $Ga_2O_3$, Appl. Phys. Lett. 112 (2018).
[15] T. Huynh, L. Lem, A. Kuramata, M. Phillips, C. Ton-That, Kinetics of charge carrier recombination in β-$Ga_2O_3$ crystals, Phys. Rev. Mater. 2 (2018) 105203.
[16] T. Onuma, S. Fujioka, T. Yamaguchi, M. Higashiwaki, K. Sasaki, T. Masui, T. Honda, Correlation between blue luminescence intensity and resistivity in β-$Ga_2O_3$ single crystals, Appl. Phys. Lett. 103 (2013).
[17] T.T. Huynh, E. Chikoidze, C.P. Irvine, M. Zakria, Y. Dumont, F.H. Teherani, E. V. Sandana, P. Bove, D.J. Rogers, M.R. Phillips, C. Ton-That, Red luminescence in H-doped β-$Ga_2O_3$, Phys. Rev. Mater. 4 (2020) 085201.
[18] S. Marcinkevičius, J.S. Speck, Ultrafast dynamics of hole self-localization in β-$Ga_2O_3$, Appl. Phys. Lett. 116 (2020).
[19] J.B. Varley, A. Janotti, C. Franchini, C.G. Van de Walle, Role of self-trapping in luminescence and p-type conductivity of wide-band-gap oxides, Phys. Rev. B 85 (2012) 081109.
[20] S. Meuret, M.S. Garcia, T. Coenen, E. Kieft, H. Zeijlemaker, M. Lätzel, S. Christiansen, S. Woo, Y. Ra, Z. Mi, Complementary cathodoluminescence lifetime imaging configurations in a scanning electron microscope, Ultramicroscopy 197 (2019) 28–38.
[21] J. Du, J. Xing, C. Ge, H. Liu, P. Liu, H. Hao, J. Dong, Z. Zheng, H. Gao, Highly sensitive and ultrafast deep UV photodetector based on a β-$Ga_2O_3$ nanowire network grown by CVD, J. Phys. D Appl. Phys. 49 (2016) 425105.
[22] H. Liang, Y. Chen, X. Xia, C. Zhang, R. Shen, Y. Liu, Y. Luo, G. Du, A preliminary study of $SF_6$ based inductively coupled plasma etching techniques for beta gallium trioxide thin film, Mater. Sci. Semicond. Process. 39 (2015) 582–586.
[23] W.-K. Wang, S.Y. Wang, Y.H. Zhang, S.-Y. Huang, Passivation effect on the surface characteristics and corrosion properties of yttrium oxide films undergoing $SF_6$ plasma treatment, Ceram. Int. 48 (2022) 19824–19830.
[24] Y. Xu, B. Bo, X. Gao, Z. Qiao, Passivation effect on ZnO films by $SF_6$ plasma treatment, Crystals 9 (2019) 236.
[25] M. Kumar, V. Kumar, R. Singh, Diameter tuning of β-$Ga_2O_3$ nanowires using chemical vapor deposition technique, Nanoscale Res. Lett. 12 (2017) 184.
[26] J. Yang, W. Zhou, J. Hu, R. Jiang, G. Sun, J. Zhao, F. Wang, F. Fang, Y. Song, D. Sun, Universal Renaissance Strategy of Metal Fluoride in Secondary Ion Batteries Enabled by Liquid Metal Gallium, Adv. Mater. 35 (2023) 2301442.
[27] C.-C. Wang, B.-C. Lee, F.-S. Shieu, H.C. Shih, Characterization and photoluminescence of Sn-doped β-$Ga_2O_3$ nanowires formed by thermal evaporation, Chem. Phys. Lett. 753 (2020) 137624.
[28] E. Polydorou, A. Zeniou, D. Tsikritzis, A. Soultati, I. Sakellis, S. Gardelis, T. A. Papadopoulos, J. Briscoe, L.C. Palilis, S. Kennou, Surface passivation effect by fluorine plasma treatment on ZnO for efficiency and lifetime improvement of inverted polymer solar cells, J. Mater. Chem. A 4 (2016) 11844–11858.
[29] B. Liu, M. Gu, X. Liu, S. Huang, C. Ni, First-principles study of fluorine-doped zinc oxide, Appl. Phys. Lett. 97 (2010) 122101.
[30] W. Yu, J.G. Lee, Y.-H. Joo, B. Hou, D.-S. Um, C.-I. Kim, Etching characteristics and surface properties of fluorine-doped tin oxide thin films under $CF_4$-based plasma treatment, Appl. Phys. A 128 (2022) 942.
[31] M. Grodzicki, Properties of bare and thin-film-covered gan (0001) surfaces, Coatings 11 (2021) 145.
[32] S. Tanuma, C.J. Powell, D.R. Penn, Calculations of electron inelastic mean free paths. V. Data for 14 organic compounds over the 50–2000 eV range, Surf. Interface Anal. 21 (1994) 165–176.
[33] C. Han, L. Mazzarella, Y. Zhao, G. Yang, P. Procel, M. Tijssen, A. Montes, L. Spitaleri, A. Gulino, X. Zhang, High-mobility hydrogenated fluorine-doped indium oxide film for passivating contacts c-Si solar cells, ACS Appl. Mater. Interfaces 11 (2019) 45586–45595.
[34] C.P. Irvine, A. Stopic, M.T. Westerhausen, M.R. Phillips, C. Ton-That, Enhancement of excitonic and defect-related luminescence in neutron transmutation doped β-$Ga_2O_3$, Phys. Rev. Mater. 6 (2022) 114603.
[35] K. Yamamura, L. Zhu, C.P. Irvine, J.A. Scott, M. Singh, A. Jallandhra, V. Bansal, M. R. Phillips, C. Ton-That, Defect Compensation in Nitrogen-Doped β-$Ga_2O_3$ Nanowires: Implications for Bipolar Nanoscale Devices, ACS Appl. Nano Mater. 5 (2022) 12087–12094.
[36] S. Yamaoka, Y. Furukawa, M. Nakayama, Initial process of photoluminescence dynamics of self-trapped excitons in a β-$Ga_2O_3$ single crystal, Phys. Rev. B 95 (2017) 094304.
[37] T. Onuma, Y. Nakata, K. Sasaki, T. Masui, T. Yamaguchi, T. Honda, A. Kuramata, S. Yamakoshi, M. Higashiwaki, Modeling and interpretation of UV and blue luminescence intensity in β-$Ga_2O_3$ by silicon and nitrogen doping, J. Appl. Phys. 124 (2018).
[38] S. Morimoto, H. Nishinaka, M. Yoshimoto, Growth and characterization of F-doped α-$Ga_2O_3$ thin films with low electrical resistivity, Thin Solid Films 682 (2019) 18–23.
[39] D. Kaur, P. Vashishtha, G. Gupta, S. Sarkar, M. Kumar, Surface nanopatterning of amorphous gallium oxide thin film for enhanced solar-blind photodetection, Nanotechnology 33 (2022) 375302.
[40] U. Varshney, A. Sharma, P. Vashishtha, L. Goswami, G. Gupta, $Ga_2O_3$/GaN heterointerface-based self-driven broad-band ultraviolet photodetectors with high responsivity, ACS Appl. Electron. Mater. 4 (2022) 5641–5651.
[41] A. Othonos, M. Zervos, C. Christofides, Carrier dynamics in β-$Ga_2O_3$ nanowires, J. Appl. Phys. 108 (2010).
[42] Z. Hu, Y. Lv, C. Zhao, Q. Feng, Z. Feng, K. Dang, X. Tian, Y. Zhang, J. Ning, H. Zhou, Beveled Fluoride Plasma Treatment for Vertical β-$Ga_2O_3$ Schottky Barrier Diode With High Reverse Blocking Voltage and Low Turn-On Voltage, IEEE Electron Device Lett. 41 (2020) 441–444.